Molecular Crystals and Liquid Crystals
Publication details, including instructions for authors and subscription information:
http://www.tandfonline.com/loi/gmcl16

Deformation and Structural Re-formation of Lyotropic Cholesteric Liquid Crystal of Hydroxypropyl Cellulose + Water System

T. Asada [a] , K. Toda [a] & S. Onogi [a]
[a] Department of Polymer Chemistry, Kyoto University, Kyoto, 606, Japan
Version of record first published: 14 Oct 2011.

To cite this article: T. Asada , K. Toda & S. Onogi (1981): Deformation and Structural Re-formation of Lyotropic Cholesteric Liquid Crystal of Hydroxypropyl Cellulose + Water System, Molecular Crystals and Liquid Crystals, 68:1, 231-246

To link to this article: http://dx.doi.org/10.1080/00268948108073566

Mol. Cryst. Liq. Cryst., 1981, Vol. 68, pp. 231–246
0026-8941/81/6801-0231 $06.50/0

Printed in the United States of America

Deformation and Structural Re-formation of Lyotropic Cholesteric Liquid Crystal of Hydroxypropyl Cellulose + Water System†

T. ASADA, K. TODA, and S. ONOGI

Department of Polymer Chemistry, Kyoto University, Kyoto 606, Japan.

(*Received July 27, 1980, in final form September 8, 1980*)

Flow properties and optical properties in applying and stopping shear on a lyotropic cholesteric liquid crystalline system of concentrated aqueous solutions of hydroxypropyl cellulose have been studied. The wave length dependence of transmitted light intensity through a sample subjected to steady shear have been measured quantitatively at various shear rates. The spectra of absorbance after the sudden cessation of steady shear flow are also observed as function of time. The shape of the spectrum at a steady state changes very much with shear rate. The shape of spectrum after the sudden cessation of steady shear always recovers quickly. A theoretical model including orientation distribution of Bragg reflection elements is proposed, which is useful to interpret observed spectra-data. Flow situations and also structural formation processes change markedly above and below a certain critical shear rate.

1 INTRODUCTION

Iridescent color assumed by cholesteric liquid crystal has been explained by Fergason[1] who assumed Bragg type reflection sites. Adams *et al.*[2] as well as Pochan and co-workers[3-5] have also explained the effect of mechanical disturbance on reflection spectra of thermotropic cholesteric liquid crystals of low molecular weights based on the same concept. Pochan and co-workers[3-5] have studied the mechanism of shear-induced structural changes in cholesteric liquid crystals,[3] cholesteric nematic mixtures[4] and cholesteric polymer blends[5] by using a unique rheo-optical technique designed by them. They measured wave length dependence of transmitted light intensity as function of applied shear rate, and interpreted the data together with rheological data.

† Presented at the Eighth International Liquid Crystal Conference, Kyoto, July 1980.

This paper intends to measure rheo-optical properties of lyotropic cholesteric liquid crystal of hydroxypropyl cellulose in water during and after steady shear flow in a similar way and to explain experimental results along these line. In the present work, however, some improvements have been made in both experimental method and analysis method of the obtained data.

2 EXPERIMENTAL

2.1 Apparatus

An experimental set-up used is similar to that reported previously by Pochan and Marsh.[3] Cone and plate geometry, however, is used instead of parallel plate, so that it is possible to apply uniform shear rate throughout the sample.

A cone and plate type rheometer equipped a transparent cone and plate made of quartz is combined with a spectrophotometer (Jasco UVIDEC-1), which was modified to measure the wave length dependence of transmitted light intensity of a sample between the cone and plate. The block diagram of the apparatus is shown in Figure 1. The standard room for the sample and reference beams was replaced with a newly designed light guide box (F). The original standard light source was replaced with a 500 W Xenon lamp house (A). The right half ($I. K. P. Q. R. S. T. U. V$) of the block diagram works as a cone-plate type rheometer. Rotation of the plate at a constant speed applies a shear on a sample at a definite shear rate. And the torque is detected by a transducer (Q), which provides us the shear stress and the viscosity. The left half of the diagram is an optical system. The standard sample beam (e) is introduced normally to the shear plate (I) by a set of prism (G_1) and glass fiber tube (H_1) and passes through a sample (J) between the plate (I) and cone (K). The transmitted light beam is introduced to the receiving sector mirror (L), through a set of glass fiber tube (H_2) and prism (G_2).

Thus, the apparatus enables us to measure simultaneously rheological properties and wave length dependence of transmitted light intensity through a sheared sample.

2.2 Material

HPC (hydroxypropyl cellulose) of weight-average molecular weight 8×10^4 was obtained from Nihonsoda Co. Ltd. Concentrated aqueous solutions ($43 \sim 68$ wt%) of this polymer form cholesteric liquid crystals at 25° C, which assume beautiful iridescent color. 61 (wt%) aqueous solution at 25°C was studied, which was ascertained to be single phase liquid crystalline solution in the quiescent state by microscopic observations and so on.

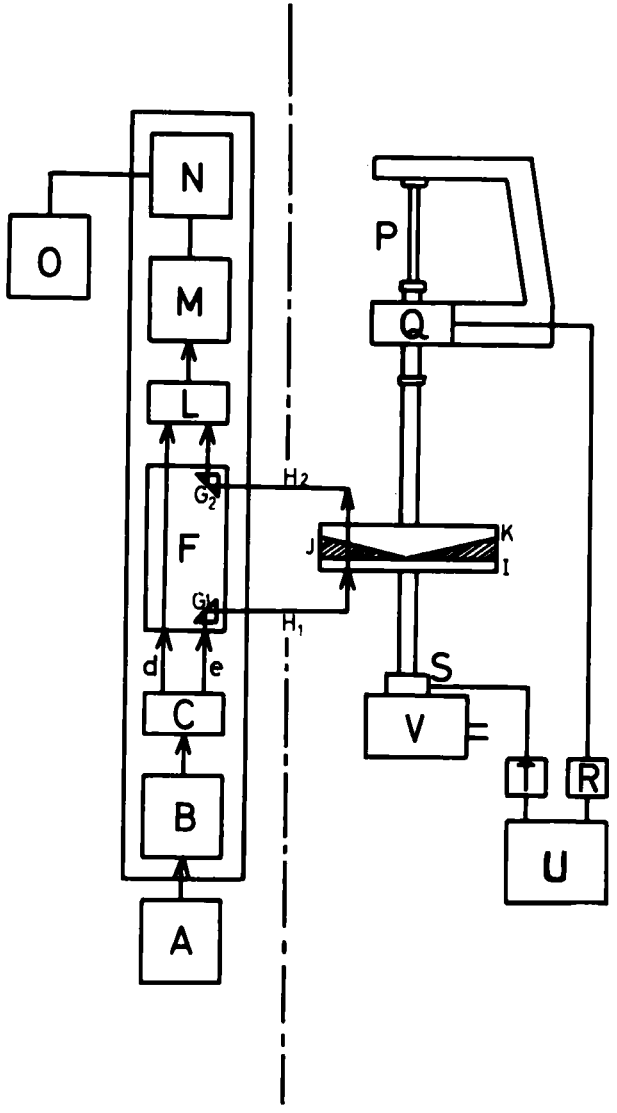

FIGURE 1 Block diagram of Rheo-optical Apparatus. The right-hand side (*I. K. P. Q. R. S. T. U. V*) represents a cone and plate rheometer. *I:* Quartz plate, *K:* Quartz cone, *P:* Torsion wire, *Q:* Differential transducer for detecting torque, *S:* Differential transducer for detecting applied strain, *V:* Gear box for driving, *T,R:* Amplifiers, *U:* Recorder. The left-hand side is an optical system. *A:* Xenon lamp, *B:* Monochrometer, *C, L:* Sector mirrors, *F:* Double beam box, *M:* Detector, *N:* Amplifier, *O:* Recorder, *e:* Sample beam, *d:* Reference beam, G_1, G_2: Prisms, H_1, H_2: Glass fiber tubes, *J:* Sample. Thick arrows show the direction of light beam propagation.

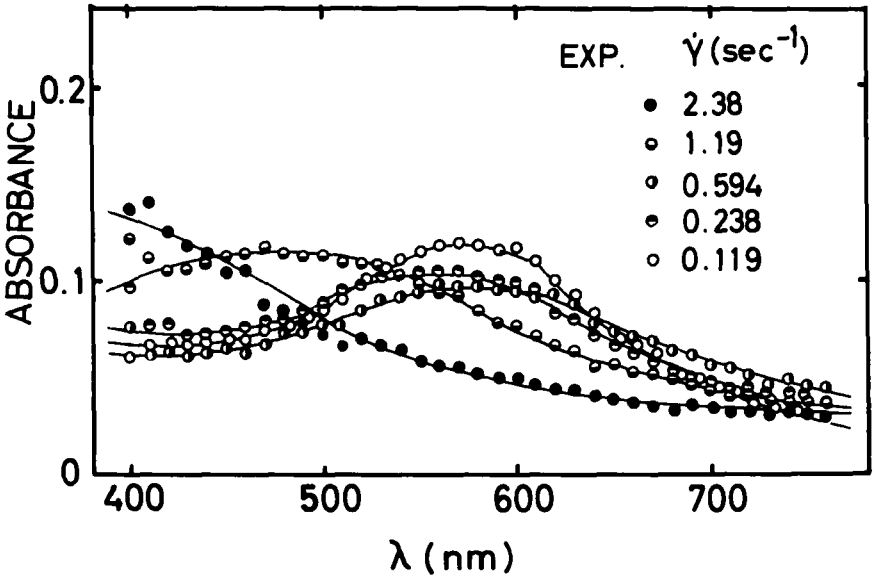

FIGURE 2 Absorbance as a function of wave length for 61(%) aqueous solution of HPC at various steady shear rates.

2.3 Measurements

Wave length dependence of transmitted light intensity through a sample subjected to shear have been measured quantitatively at various shear rate ($1.2 \times 10^{-1} \sim 2.4\,s^{-1}$). The spectra of absorbance after the sudden cessation of steady shear flow are also observed as function of time.

The slit function of the spectrophotometer was a triangular one, the half-value width of which was less than 0.5 nm over the experimental wave length range (400 ~ 760 nm). When the experimental data were compared with calculated data (computer-fit treatment), the slit function was also taken into account.

A cone with a cone angle 1.01° was used. The diameters of cone and plate were 80 mm. The direction of light propagation was always normal to the plate. The thickness of the sample at the position where the light beam passed through is 0.44 mm. Arc shaped slits with 2 mm width and 10 mm length were used on both the entrance and the exit sides. The circle of the arc of a slit was coaxial with the rotational axis of the plate and was 25 mm apart from the rotational axis of the plate. To keep the experimental condition to be constant, cone and plate were rubbed always tangentially with a sheat of qualified gauze beforehand.

3 RESULTS and DISCUSSION

3.1 Preliminary experimental results

The spectrum of transmitted light changes with time during shear application at constant rate, until it reaches a steady state value. In Figure 2 the steady-state spectrum obtained at various shear rates is shown. As is seen from the figure, the shape of the spectrum in the steady state changes with shear rate. The wave length λ_M at which a maximum is observed shifts to the blue side with increasing shear rate.

When the shear is stopped suddenly, the spectrum recovers quickly. In Figure 3, is shown as an example the recovery of the spectrum for the case $\dot{\gamma} = 1.19$

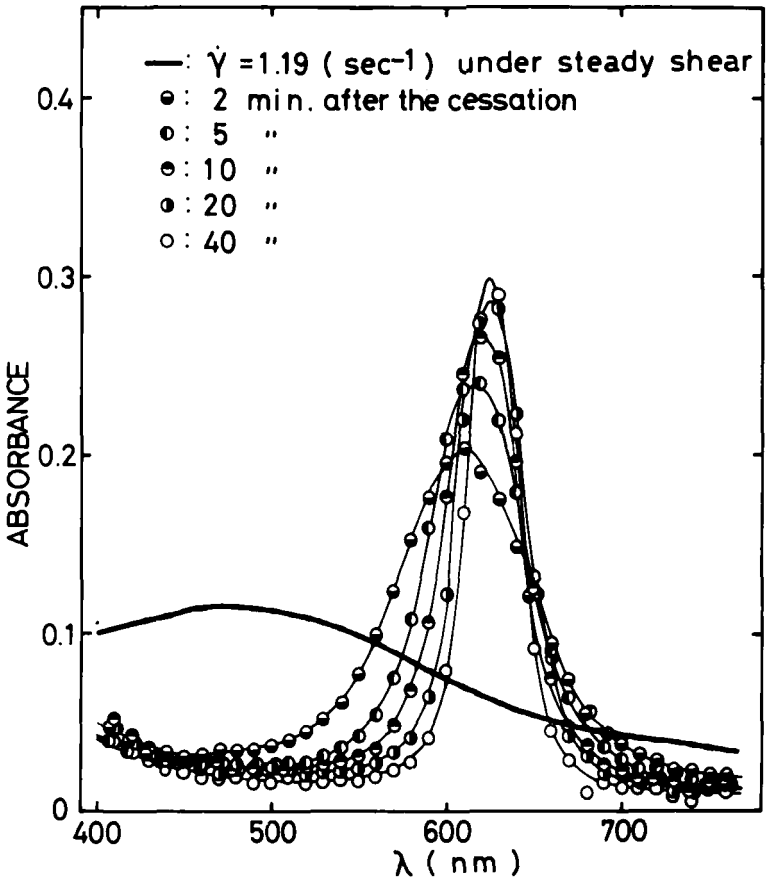

FIGURE 3 Recovery of spectrum, after the cessation of the steady shear flow ($\dot{\gamma} = 1.19\,s^{-1}$). The solid line shows the spectrum at the steady state shear flow.

s^{-1}, after the sudden cessation of steady flow. In the figure, the solid curve represents the spectrum at the steady state shear flow, which is very broad in shape. When the shear is stopped, however, the shape of the spectrum becomes very sharp within two minutes. The spectrum becomes sharper and sharper with time. After a certain time, λ_M does move no longer and only the height of spectrum grows with time. Eventually the sample becomes very transparent and seems to achieve a Grandjean-like texture.

3.2 A model for calculating the absorbance spectrum

The optical data shown above may be interpreted well by assuming disorientation of Bragg sites during steady flow and their re-orientation after cessation of the flow, as suggested before by Pochan and co-workers[3-5] for low molecular weight cholesteric materials. A certain type of orientation distribution function of Bragg reflection elements will be introduced in this paper, for convenience of further discussion depending on current concept of cholesteric reflection such as shown by Chandrasekhar *et al.*[6]

Let us consider small orientation elements which act also as Bragg sites and satisfy the following assumptions:

(i) The intensity distribution against wave length of the reflection light for a single "Bragg element" is Lorentzian with respect to $\lambda_0 = \bar{n}P_0$, where P_0 is the cholesteric pitch and $\bar{n}$ is the refractive index of the matrix.

(ii) The distribution of the orientation of Bragg elements is represented approximately by rotational symmetric distribution of Gaussian type with respect to a certain orientation reference axis (OZ).

As is shown in Figure 4, the experimental result for a Grandjean-like texture of HPC liquid crystal 40 min. after the cessation of steady flow can be computer-fitted by assuming that the reflection curve from each Bragg element is Lorentzian. Such a result of computer-fitting and theoretical results reported by Chandrasekhar *et al.*[6] for finite thickness of Bragg elements may support the adequacy of the assumption (i). The assumption (ii) is partly based on some experimental knowledge obtained by microscopic observations that HPC molecules are easy to align on the glass wall; due to the wall effect, cholesteric structure always grows so as that its optical axis is normal to the glass wall.

Now, we will consider the case in which the orientation axis (reference axis) is normal to the plate, i.e. the orientation axis is parallel to the direction of light propagation. From the assumption (i), the wave length dependence curve of absorbance $f(\lambda)$ for a Grandjean texture whose optic axis is parallel with the direction of light propagation (cf. Figure 5a) can be represented by

$$f(\lambda) = \frac{C \cdot B}{(\lambda - \lambda_0)^2 + B^2} \tag{1}$$

and

$$\lambda_0 = \bar{n} P_0 \tag{2}$$

where λ, P_0 and $\bar{n}$ are, respectively, wave length, the cholesteric pitch and the mean refractive index. B is the half-value width of Lorentzian curve. C will be proportional to the number of Bragg elements for simple systems.

When the axis of the element is tilting from the orientation axis by an angle of θ (as is shown schematically in Figure 5b), the wave length dependence curve of the absorbance $f(\lambda)$ should be given by;

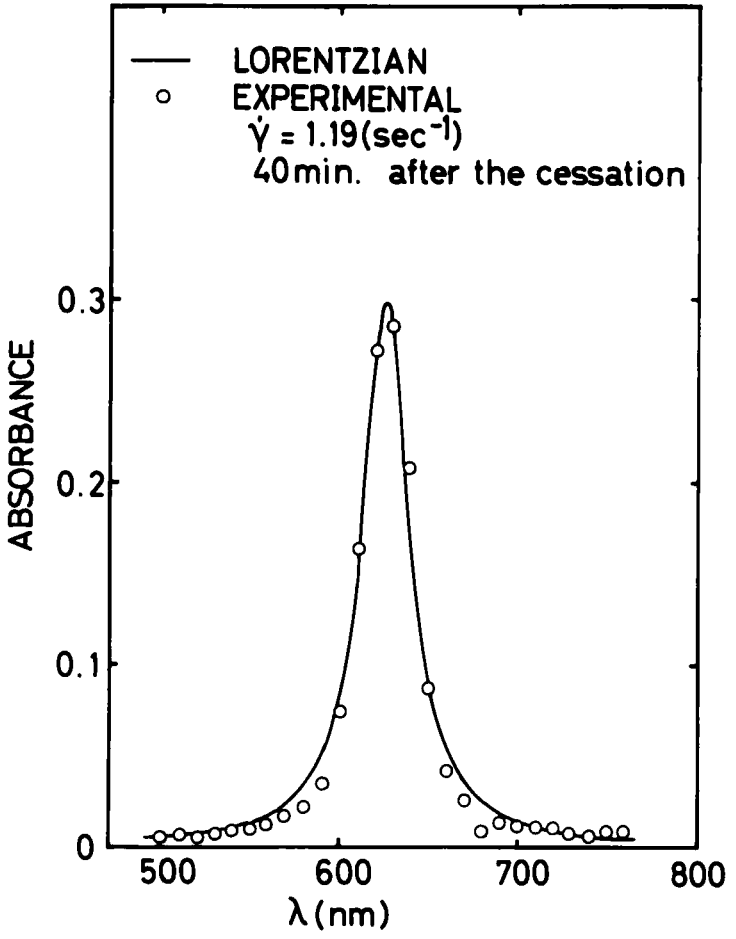

FIGURE 4 Computer-fitting based on the assumption (1). Open circles are the experimental results for a Grandjean-like texture.

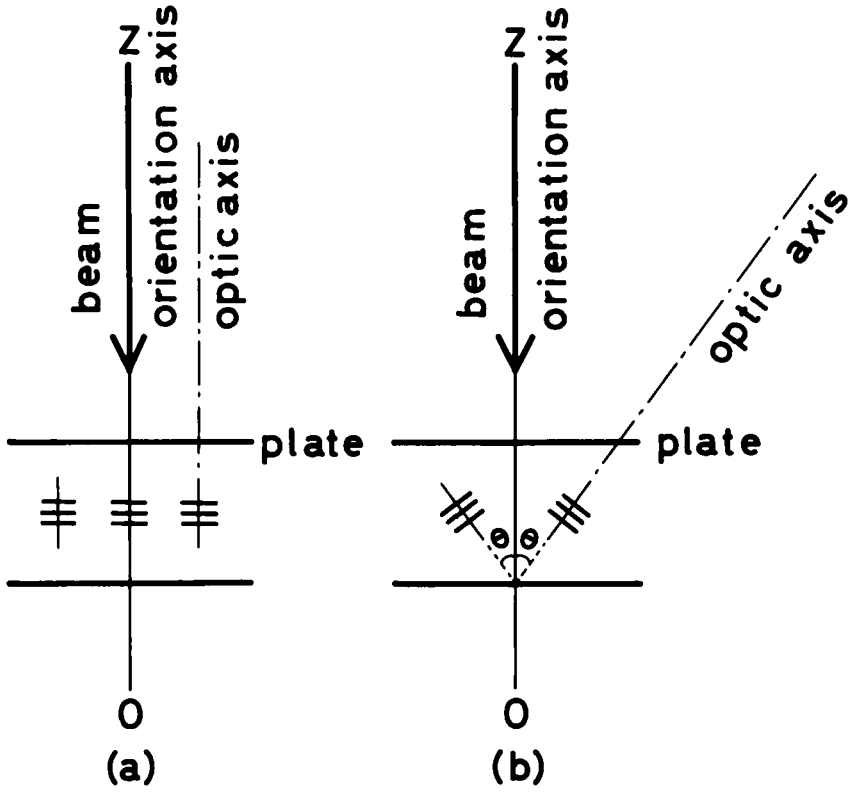

FIGURE 5 Geometry for cholesteric Bragg elements and an orientation axis (OZ). Incident light is shown by a thick arrow. (a) Helical screw axis of a cholesteric Bragg element is normal to the plate. (b) Helical screw axis is at angle θ from the normal.

$$f(\lambda) = \frac{C \cdot B \cos\theta}{(\lambda - \lambda_0 \cos\theta)^2 + B^2 \cos^2\theta} \tag{3}$$

and

$$\lambda_M = \lambda_0 \cos\theta \tag{4}$$

where λ_M is the wave length at which the spectrum has a maximum. When $\theta = 0$, the Eq. (3) reduces to Eq. (1), and $\lambda_M = \lambda_0$.

From the assumption (ii), the orientation distribution function or the probability $F(\theta)$ for elements whose optic axes are at angle θ from the orientation axis (OZ), which is parallel to the direction of light propagation, is given by

$$F(\theta) = \frac{\sin\theta \exp(-D^2\theta^2)}{\int_0^{\pi/2} \sin\theta \exp(-D^2\theta^2) d\theta} \tag{5}$$

where D is a parameter to determine the sharpness of the orientation distribution. The reciprocal of D is analogous to the standard deviation in a Gaussian distribution.

Combining Eq. (3) and Eq. (5), we obtain the following equation, which enable us to calculate the wave length dependence of the absorbance:

$$\log (I_0/I) = \int_0^{\pi/2} \frac{C \cdot B \cos\theta \, F(\theta)}{(\lambda - \lambda_0 \cos\theta)^2 + B^2 \cos^2\theta} d\theta + \frac{E}{\lambda^4} \qquad (6)$$

The second term of the right-hand side of Eq. (6) represents the base line of the spectrum.

Figure 6 shows an example of results of computer calculations of Eq. (6). In this particular case, λ_0, B, and C were kept constant as are indicated in the figure, and only D was changed from 0 to 4. It is clear from the figure that the calculated absorption spectrum drastically changes its shape with D. It becomes sharper as D increases.

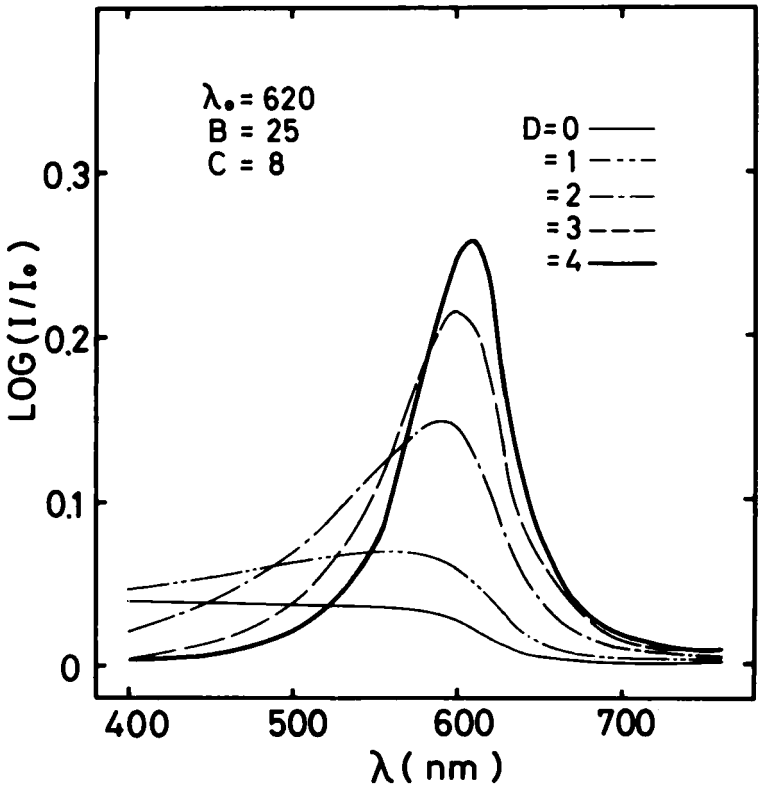

FIGURE 6 Calculated wave length dependence of absorbance by Eq. (5). An example when only parameter D changes is shown.

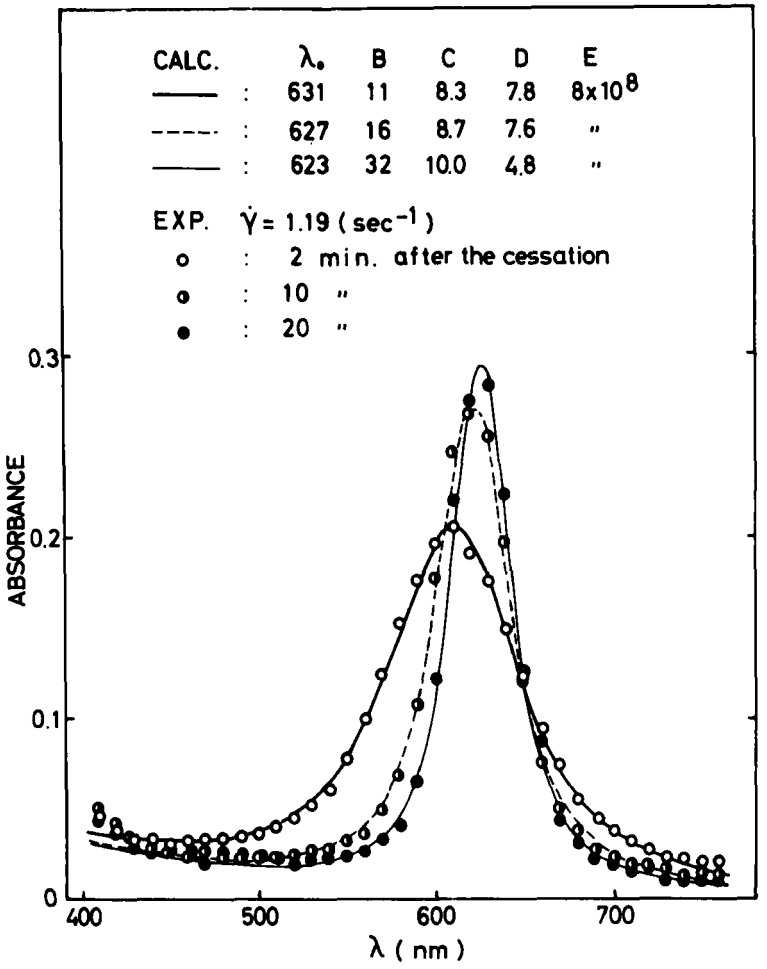

FIGURE 7 Computer-fitting by using Eq. (5) for the experimental results after cessation of steady shear flow ($\dot{\gamma} = 1.19\ s^{-1}$). Parameters are listed on the figure.

3.3 Results for structural formation processes

The equation introduced above is helpful for discussing a process of structure formation of cholesteric liquid crystals. Figure 7 gives an example of computer-fitting to the experimental result shown in Figure 3 for the structural formation process after the cessation of steady shear flow. As is evident from the figure, calculated values (lines) coincide with experimental ones (circles) very well, when suitable values are assumed for the parameters in the above equations. The change in the shape of spectrum with time will be discussed in terms of the change in the parameters, hereafter.

As is shown in Figure 8, parameter B decreases rapidly with time after the cessation of steady shear flow. It is noteworthy that when the sample experienced low shear rates (0.119 and 0.238 s^{-1}) B becomes higher. Furthermore, the higher the experienced shear rate is, the more rapidly B decreases. From this result, it follows that the higher the experienced shear rate is, the more rapidly and more completely the cholesteric structure re-forms after the cessation of the steady flow. Figure 9 shows the variation of D, the sharpness of the orientation distribution, with time. At low shear rates below 0.594 s^{-1}, the orientation distribution does not change with time, while at higher shear rates D increases rapidly with time. It is interesting to note that the shear rate region, where D does not change with time, corresponds to the yielding region of the flow curve, where the apparent viscosity increases with decreasing rate of shear.

In Figure 10, the apparent viscosity is plotted against rate of shear. This viscosity curve can be divided into two regions, the yielding region at lower rate and the Newtonian region above a certain critical rate of shear $\dot{\gamma}_c$, neglecting the shear-thinning region observed at the high shear-rate end. Below the critical shear rate $\dot{\gamma}_c$, the sample probably flows retaining some superstructure, in which many elements are packed in regular manner. Under such circumstances, Bragg elements hardly can re-orient themselves, even after the

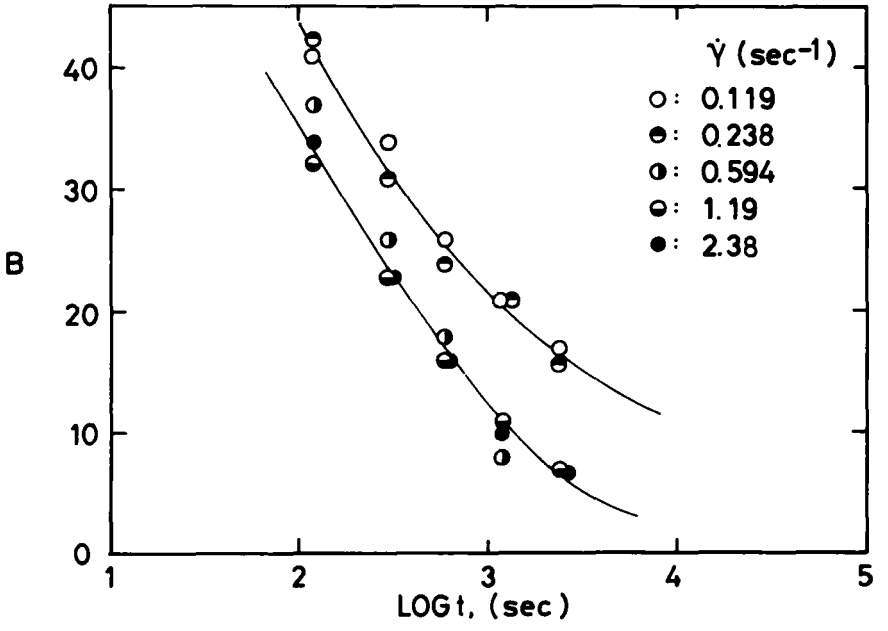

FIGURE 8 The parameter B as a function of time, for various experienced shear rates.

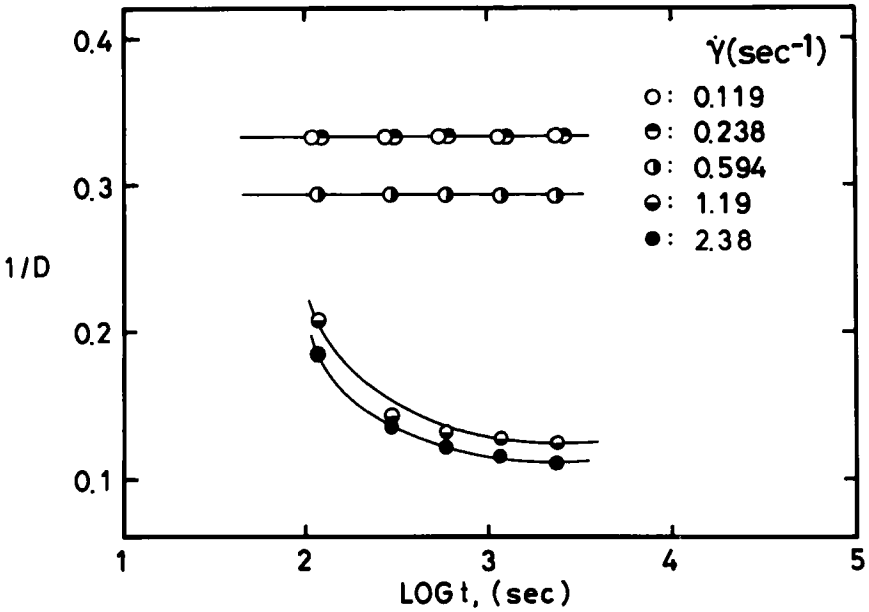

FIGURE 9 The reciplocal of D, the broadness of orientation distribution, as a function of time for various experienced shear rates.

cessation of steady shear flow. On the other hand, above the critical shear rate, superstructure may be disintegrated to smaller flow units, which are expected to be as small as Bragg elements. Thus, when the perturbation by shear is ceased, these elements can re-orient very rapidly and very neatly. Consequently, the uniformity of the orientation of Bragg elements can be improved to show intensive increase in D with time.

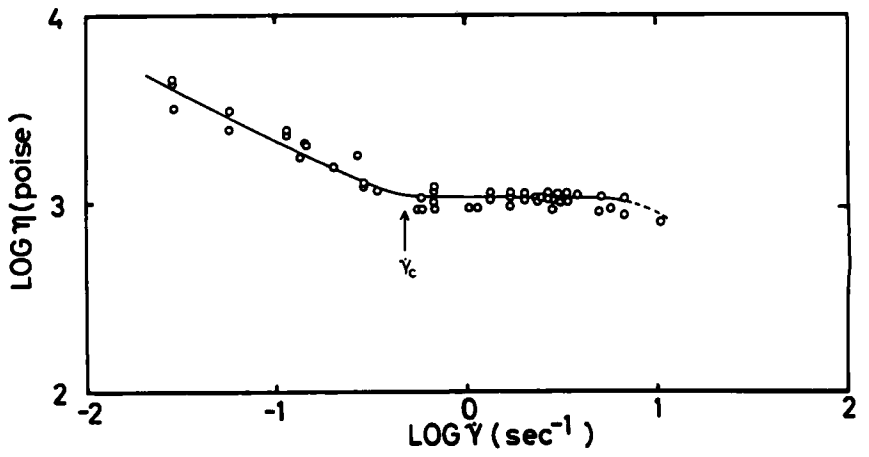

FIGURE 10 Apparent viscosity as a function of shear rate ($\dot{\gamma}$).

3.4 Results for steady shear flow

As shown in Figure 2, the shape of spectrum observed during steady shear flow depends upon rate of shear. The spectrum becomes broader, and λ_M (the wave length at the peak) shifts to the blue side with increasing rate of shear. Above a certain shear rate, the shifting of the peak becomes extremely large. Such blue shift of the peak with increasing rate of shear also observed by Pochan *et al.*[3] for thermotropic cholesteric liquid crystals of low molecular weight materials. They attributed the blue shift of the peak mainly to the tilting of the Bragg elements. It seems, here, also that tilting of the orientation axis due to shearing force should be taken into account, to interpret these phenomena satisfactorily.

When the orientation axis tilts by an angle of θ_0, as schematically shown in Figure 11, Eq. (6) becomes as follows:

$$\log (I_0/I) = \int_0^{\pi/2} d\theta \int_0^{2\pi} \frac{C \cdot B \cos x \cdot F(\theta)}{(\lambda - \lambda_0 \cos x)^2 + B^2 \cos^2 x} d\psi + \frac{E}{\lambda^4} \qquad (7)$$

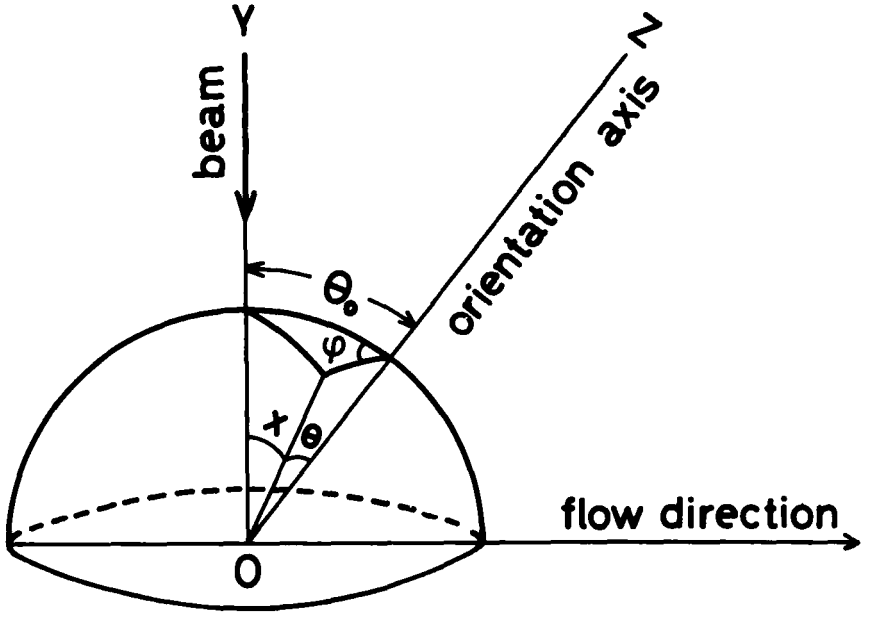

FIGURE 11 Geometry that orientation axis (OZ) is at angle θ_0 from the normal. Incident light is shown by a thick arrow. The direction of an optic axis of a Bragg element is determined by (θ_0, θ, ψ).

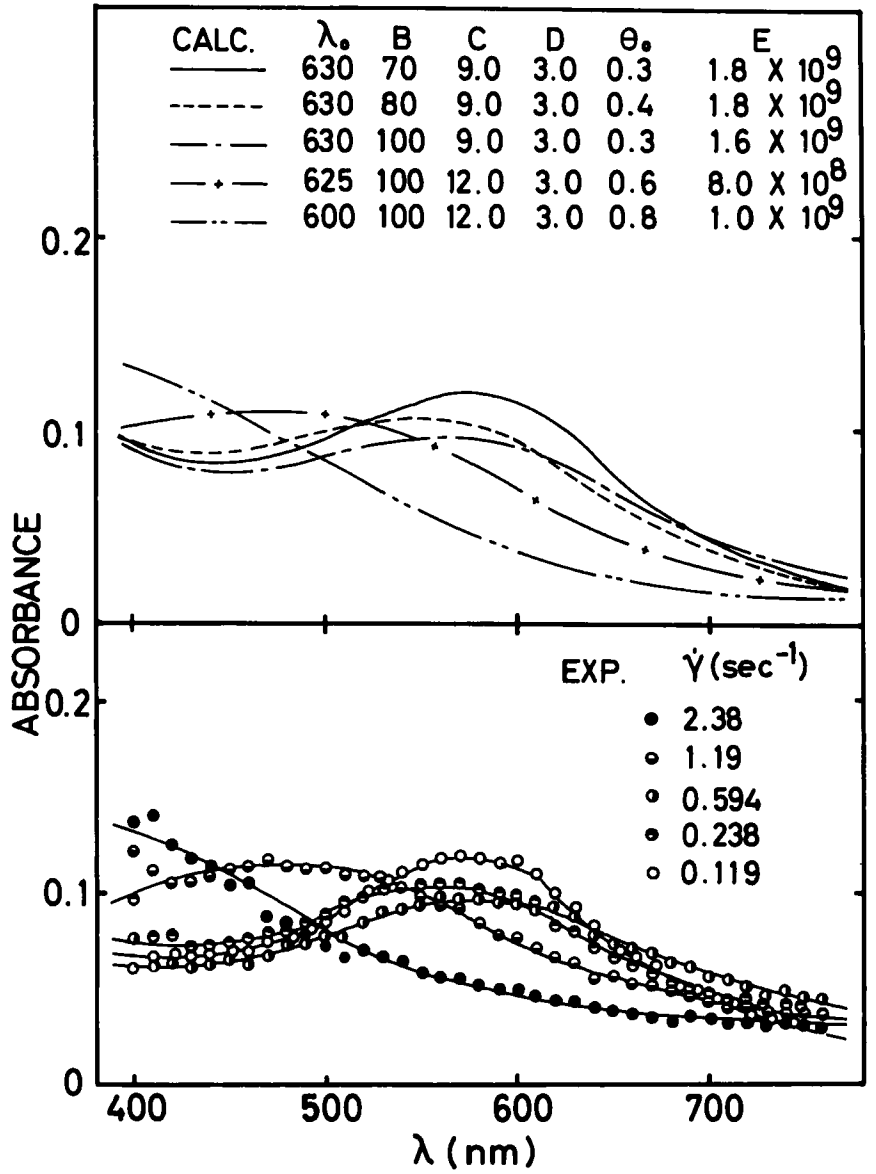

FIGURE 12 Computer-fitting results using Eq. (6) for the results of steady shear flow. In the top are shown the calculated curves. The parameters are listed on the top figure, where θ_0 is the tilting angle of orientation axis in radian. In the bottom are shown experimental results.

where

$$F(\theta) = \frac{\sin\theta \exp(-D^2\theta^2)}{\int_0^{\pi/2} \sin\theta \exp(-D^2\theta^2) d\theta}$$

$$\cos x = \cos\theta_0 \cos\theta + \sin\theta_0 \sin\theta \cos\psi$$

From this equation, the wave length dependence of absorbance can be calculated. At the top in Figure 12, results of computer-fitting to experimental curves (bottom of Figure 12 or Figure 2) obtained during the steady shear flow are shown. Numerical values employed for parameters are also indicated in the same figure. The tilting angle θ_0 in radian is almost unchanged at low shear rates, while it changes very much at high shear rates or in the Newtonian region. As described before, in this high shear-rate region, superstructure is disintegrated into smaller flow units. These units can easily be oriented so as that their optic axes are parallel to a direction somewhat tilted from the normal, because of their small size. When the shear flow is ceased, the units orient so as their optic axes are normal to the surface of the plate. This process is the structure formation process discussed before.

Highly oriented Grandjean-like texture can be attained only by the re-orientation of smaller flow units after cessation of shear flow, and for it, liquid crystals should be flowed at shear rates higher than the critical shear rate.

Similarity also reported by Pochan *et al.*[3] for low molecular weight cholesteric system that tilting angle of Bragg element became greater in the Newtonian flow region. More detailed investigations involving other rheo-optical method,[7] however, seems to be necessary, before judging whether the proposed flow mechanism by Pochan *et al.*[3] for low molecular weight system is applicable to this polymeric system too or not.

Concluding Remarks

Using cone-plate geometry, it becomes possible to measure and to compare both the optical data and the rheological data on the same condition.

Setting a model for calculation makes it possible to discuss more quantitatively orientational change and structural change of cholesteric structure separately. In the present case, the re-formation process was rather slow and was able to be observed more finely, so that we can discuss the flow mechanisms from the study of reformation processes too. There still remains, however, to clarify the physical meaning of the parameters B and D in more details based on the current molecular theories. After that, the analyses of the spectra-data for formation process may relate kinetics of structural formation.

References

1. J. L. Fergason, *Mol. Cryst.*, **1**, 293 (1966).
2. J. E. Adams, W. Haas and J. Wysocki, *J. Chem. Phys.*, **50**, 2458 (1969).
3. J. M. Pochan and D. G. Marsh, *J. Chem. Phys.*, **57**, 1193 (1972).
4. D. G. Marsh and J. M. Pochan, *J. Chem. Phys.*, **58**, 2835 (1973).
5. D. G. Marsh, J. M. Pochan and P. F. Erhardt, *J. Chem. Phys.*, **58**, 5795 (1973).
6. S. Chandrasekhar and J. S. Prasad, *J. Mol. Cryst. Liq. Cryst.*, **14**, 115 (1971).
7. T. Asada, H. Muramatsu, R. Watanabe and S. Onogi, Macromolecules, in press.